On the interplay of solvent and conformational effects in simulated excited-state dynamics of a copper phenanthroline photosensitizer

Gianluca Levi,*[a] Elisa Biasin,[b‡] Asmus O. Dohn,[a] and Hannes Jónsson[a]

Copper(I) bis-phenanthroline complexes represent Earth-abundant alternatives to ruthenium-based sensitizers for solar energy conversion and photocatalysis. Improved understanding of the solvent-mediated excited-state structural dynamics can help optimize their photoconversion efficiency. Through direct dynamics simulations in acetonitrile and excited-state minimum energy path calculations in vacuum, we uncover the mechanism of the photoinduced flattening motion of the prototypical system $[Cu(dmphen)_2]^+$ (dmphen=2,9-dimethyl-1,10-phenanthroline). We find that the ligand distortion is a two-step process in acetonitrile. The fast component (∼110 fs) is due to spontaneous pseudo Jahn-Teller instability and is largely solvent independent, while the slow component (∼1.2 ps) arises from the mutual interplay between solvent molecules closely approaching the metal center and rotation of the methyl substituents. These results shed new light on the influence of a donor solvent like acetonitrile and methyl substituents on the flattening dynamics of $[Cu(dmphen)_2]^+$.

1 Introduction

Copper(I) bis-phenanthroline complexes can be efficiently excited by UV-vis light to metal-to-ligand charge transfer (MLCT) states with electron-donating abilities; thus they have the potential to compete with the currently most promising ruthenium(II) polypiridines as sensitizers in photocatalytic applications such as dye-sensitized solar cells (DSSCs) [1–4] and light-driven hydrogen production [5]. Unlike Ru photosensitizers, Cu(I) bis-phenanthroline complexes are highly flexible. The ultrafast structural dynamics in the MLCT states involve a large distortion, a flattening of the ligands (see Figure 1) from the tetrahedral coordination at the Franck-Condon (FC) geometry (near D_{2d} symmetry) to a quasi-square planar configuration (D_2). The flattening is promoted by the pseudo Jahn-Teller (PJT) instability that is characteristic of tetracoordinated Cu(II) (d^9) centers [4,6–8]. It is known [2,9–11] that this angular distortion strengthens the interaction between solvent molecules and the metal, and lowers the energy gap to the ground state, thus shortening the MLCT lifetime. A shorter MLCT lifetime can complicate the use of Cu(I) complexes as photosensitizers [2,12,13]. The excited-state lifetime can be pro-

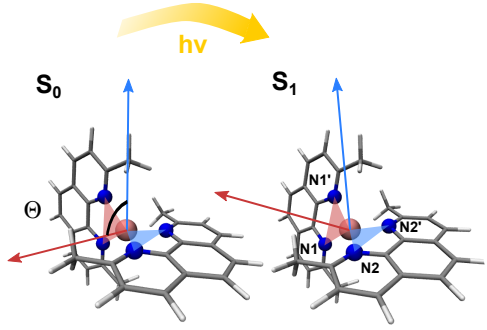

Fig. 1 Cu(I) bis-phenanthroline complexes undergo a flattening of the ligands when photoexcited. This photoinduced structural change is represented schematically for the prototypical compound investigated in the present work: $[Cu(dmphen)_2]^+$ (dmphen=2,9-dimethyl-1,10-phenanthroline). In the ground state (S_0) the ligands are nearly perpendicular to each other, while in the lowest singlet MLCT excited state (S_1) the molecule is flattened, as illustrated by the reduction in the angle Θ between the normals to the N1-Cu-N1′ and N2-Cu-N2′ planes (blue and red vectors). Color code for the atoms: Cu=pink, N=blue, C=grey, H=white.

[a] *Science Institute and Faculty of Physical Sciences, University of Iceland, 107 Reykjavík, Iceland. E-mail: giale@hi.is*

[b] *PULSE Institute, SLAC National Accelerator Laboratory, Menlo Park, California 94025, USA.*

† Electronic Supplementary Information (ESI) available: Cartesian coordinates and selected structural parameters of the gas-phase optimized geometries of $[Cu(dmphen)_2]^+$, properties of the electronic structure (excitation energy, molecular orbitals, electron density difference), parameters and residuals of the fittings, details on the generation of initial conditions for the excited-state QM/MM BOMD simulations, ground-state polar distribution of methyl dihedral angles, description of the implementation of the acetonitrile force field in ASE (PDF).

longed by ligand substitution to inhibit the torsional motion and the solvent accessibility to the Cu center[13–16]. However, major advancements in the systematic design of photofunctional Cu(I) bis-phenanthrolines are still impeded by our incomplete knowledge of the flattening mechanism, and the factors influencing it.

Here, atomistic simulations are used to resolve key mechanistic aspects of the ultrafast structural dynamics in the lowest singlet MLCT excited state (S_1) of the archetype of this class of complexes, $[Cu(dmphen)_2]^+$ (dmphen=2,9-dimethyl-1,10-phenanthroline), (see Figure 1) in acetonitrile solution. This compound has been the object of extensive experimental investigations using femtosecond optical[6,7,17–20] and X-ray absorption spectroscopy[10,20–22]. These experimental measurements have led to a characterization of the time scales of the excited-state relaxation in solution. Photoexcitation can occur directly to S_1[6,21] or to a higher energy singlet MLCT state[7,17,19], depending on the excitation wavelength used in the experiment. In case of photoexcitation to a high-lying MLCT state, S_1 is populated in less than 100 fs through fast internal conversion (IC) processes[7,19]. The experimentally deduced time constants for the PJT distortion lay within a range 100-800 fs[6,7,17,19], while population of the lowest triplet MLCT state happens in 7.4-15 ps[6,7,17,19].

Chen and co-workers[19] and the group of Tahara[6,7,15,18], and more recently the group of Castellano[17], have independently performed femtosecond transient absorption and fluorescence upconversion measurements, providing important information about the excited-state dynamics of $[Cu(dmphen)_2]^+$. On one hand, from the analysis of Chen *et al.*[19] of fluorescence upconversion data in acetonitrile the flattening dynamics appears as a prompt and spontaneous process, driven by the PJT instability at the perpendicular structure in the FC region. The same view of the flattening process emerges from the analysis of transient absorption spectra of $[Cu(dmphen)_2]^+$ in dichloromethane by Castellano *et al.*[17]. On the other hand, Tahara *et al.*[6,7,15,18] have proposed the presence of a small but finite energy barrier between the perpendicular and flattened geometries in the lowest ^{1}MLCT state. These authors suggest that the complex is in a metastable precursor state in a shallow minimum at the S_1 perpendicular geometry before the structural distortion, which is not what expected based on the picture of spontaneous flattening due to PJT instability. This theory is supported by the observation that the dampening time of coherent oscillations in the transient absorption spectrum measured in dichloromethane is similar to the time constant of the spectral change attributed to the flattening[6,18]. Besides, Tahara *et al.*[15,18,23] were the first to realize that the flattening motion must be coupled with the rotation of the methyl groups at the 2,9 positions on the phenanthroline ligands. Indeed, rotation of the substituents is expected to lower the steric hindrance at the flattened geometry, making it possible to reach the minimum energy structure in the S_1 state. The coupling explains the observation from ultrafast optical measurements that the flattening is slower for $[Cu(dmphen)_2]^+$ compared to its parent compound $[Cu(phen)_2]^+$, which does not have substituents on the ligands[15,18,23]. Finally, Chen and co-workers[19] and Tahara *et al.*[7] have characterized the time scale of the flattening in acetonitrile (the solvent of the present study) by femtosecond fluorescence spectroscopy. Both groups have identified one time constant, the decay time deduced by Tahara *et al.*[7] (340 fs) being longer than the one reported by Chen *et al.*[19] (∼100 fs).

The ultrafast optical studies of Chen and co-workers[19], Tahara *et al.*[6,7,15,18], and Castellano *et al.*[17] show that the solvent has little influence on the excited-state relaxation at early times following photoexcitation. On the other hand, it has long been recognized that interactions between solvent molecules and the exposed metal center at the flattened geometry in the excited state is responsible for shortening the lifetime of the lowest ^{3}MLCT excited state in donor (Lewis basic) solvents such as acetonitrile (∼1.6 ns[19,20]) compared to nondonor solvents such as dichloromethane (∼90 ns[17]) or toluene (∼100 ns[24]). Initially, quenching of the excited-state lifetime in acetonitrile was interpreted as a consequence of coordination of a solvent molecule to Cu to form a solute-solvent exciplex[25–27]. Chen *et al.*[20] supported this argument using results from picosecond time-resolved X-ray absorption measurements. However, the interpretation of the experimental data was not fully in line with DFT geometry optimizations of an adduct formed by the flattened complex in the MLCT state and one acetonitrile molecule. Later, Penfold *et al.*[10] demonstrated that the transient absorption spectra of $[Cu(dmphen)_2]^+$ in acetonitrile and dichloromethane are identical and can be modeled using solely the ground- and excited-state gas-phase optimized structures of the complex. Based on these observations, they concluded that no exciplex is formed in the MLCT excited state in acetonitrile. This result was supported by classical and QM/MM MD simulations showing that acetonitrile molecules can approach the metal center only for short intervals of time and at distances between 3.5 and 4 Å[10]. This weak interaction between Cu and acetonitrile molecules is sufficient to induce a stabilization of the MLCT state and therefore a faster decay to the ground state[10]. Recent X-ray transient absorption measurements by Kelley *et al.*[22] have confirmed the lack of solvent coordination in the MLCT state. Notably, no theoretical studies so far have addressed the influence of the transient approach of solvent molecules on the flattening dynamics.

Recently, Du *et al.*[28] and Capano *et al.*[29] have separately reported nonadiabatic trajectory surface hopping (TSH) dynamics simulations of photoexcited $[Cu(dmphen)_2]^+$. In both cases, the complex was described using density functional theory (DFT) and the nonadiabatic trajectories were started from a singlet excited state higher in energy than S_1. Du *et al.*[28] performed the simulations in vacuum for up to 1 ps, starting from a Wigner distribution of the first vibrational level of the ground state (sampling at 0 K). These calculations showed that decay to S_1 through IC processes proceeds very rapidly in less than 100 fs, as also observed experimentally in solution[7,19]. Flattening of the ligands was shown to start around

200 fs, well after IC to S_1. A correlation between the evolution of the dihedral angle associated with the flattening and motion of the methyl groups was noted. Besides, a time constant of ∼700 fs for the flattening distortion was deduced from the evolution of the distribution of the flattening angles. This time scale was obtained by assuming that relaxation along the flattening coordinate is completed around 500 fs after the beginning of the flattening. However, due to the form of the potential in S_1 and the lack of damping by the solvent, long-lived coherent oscillations of the flattening angles are expected to be observed in vacuum[30], which was not taken into account by the authors. Furthermore, since the simulations were performed in vacuum, the effect of the solute-solvent interactions on the flattening dynamics in the excited state could not be taken into account. Capano *et al.*[29] performed the simulations in acetonitrile using a QM/MM framework, and collected 9 trajectories, each having a length of 100 fs. The calculations confirmed the time scale of the IC processes that lead to relaxation to the S_1 state, but the trajectories were too short and the amount of MD data too little to investigate the time scale of the structural relaxation and the influence of the solvent on the flattening dynamics.

Quantum dynamics simulations on excited-state potential energy surfaces of $[Cu(dmphen)_2]^+$ computed with linear response time-dependent (TD) DFT in vacuum have also been reported[21,31]. One of the main observations from these simulations is that that intersystem crossing (ISC) to ^{3}MLCT states can occur simultaneously to the PJT distortion. This can complicate the identification of spectral changes due to the flattening in optical experiments[6,32,33]. On the other hand, the flattening dynamics is not significantly affected by such ISC events owing to similarities in the geometries of the lowest-lying singlet and triplet excited-states[21,31,34]. Therefore, in our simulations we neglect singlet-triplet transitions and focus exclusively on the structural relaxation in the S_1 state.

In this contribution, we seek to provide a mechanistic picture of the ultrafast photoinduced flattening of $[Cu(dmphen)_2]^+$ in acetonitrile by answering the following questions: Does the response of the solvent to photoexcitation of the complex influence the flattening dynamics? Is there an interplay between the response of the solvent and the rotation of the methyl groups in determining the final magnitude and time scale of the flattening distortion? Shedding light on these issues requires advancing previous computational studies by simulating a long enough time interval to describe solvent reorganization and including solvent effects explicitly. In order to do so, we perform nonequilibrium direct Born-Oppenheimer molecular dynamics (BOMD) simulations of the complex in the S_1 state in acetonitrile over more than 1 ps. The calculations include the solvent within a quantum mechanics/molecular mechanics (QM/MM) electrostatic embedding framework, and a number of trajectories have been collected starting from a thermal distribution of configurations at 300 K to obtain proper statistical sampling. The nonadiabatic TSH simulations of Capano *et al.*[29] show that after the trajectories have reached the S_1 state, no re-crossings with higher-lying singlet excited states occur during the dynamics. This is because S_1 is separated from the higher MLCT states by around 0.1 eV, as shown from TDDFT with hybrid functionals[28,34], which is well above the average thermal energy accessible to the system at 300 K (k_bT=0.0257 eV). Therefore, the BO approximation can be safely applied to investigate the structural dynamics in the S_1 state.

In addition, we compute the excited-state minimum energy path (MEP) between the perpendicular and flattened geometries. By finding the MEP in the S_1 state we test the presence of an energy barrier, while exploring the nature of the coupling between the flattening and the rotation of the methyl substituents.

2 Computational methods

In all calculations, the electronic structure of the complex is computed with DFT employing the exchange-correlation functional BLYP[35,36]. Kohn-Sham orbitals are represented with tzp and dzp localized basis sets[37] for Cu and the rest of the atoms, respectively. We choose BLYP as it has been used in previous QM/MM studies[10] of $[Cu(dmphen)_2]^+$ and its performance with respect to the structure of Cu(I) bisphenanthroline compounds is known[9,29] to be similar to more accurate but more expensive functionals including exact exchange, such as B3LYP. The calculations are performed within the Grid-based Projector Augmented Wave (GPAW) code[38,39]. The GPAW simulation cell has a grid spacing of 0.18 Å. We tested that the optimized geometry of the complex is converged with respect to the choice of grid and basis set size. Excited-state calculations employ a ΔSCF method implemented for direct dynamics simulations of metal complexes in solution[40–42]. The electronic configuration of S_1 is achieved by promoting an electron from the HOMO to the LUMO of S_0 within the spin-unpolarized formalism[43], and by applying Gaussian smeared constraints to the orbital occupation numbers. The Gaussian constraints have a width of 0.01 eV. As shown in section 2 of the ESI, at the FC geometry, the character of the electronic transition involves excitation of an electron from the nearly degenerate HOMO-1 and HOMO orbitals, with prevalent character of d_{xz}/d_{yz} metal orbitals, to the nearly degenerate LUMO and LUMO+1 orbitals, with character of π^* ligand orbitals. This is taken into account by the Gaussian smearing adopted in the ΔSCF description of the electronic excitation, which ensures that for promotion of an electron from the HOMO to the LUMO, degenerate HOMO-1/HOMO orbitals are equally depopulated (change in occupation by -0.5) while degenerate LUMO/LUMO+1 orbitals are equally populated (by +0.5).

For the direct QM/MM BOMD simulations the electrostatic embedding scheme[44] available in the Atomic Simulation Environment (ASE)[45,46] is used to interface GPAW with an empirical pairwise interaction potential for acetonitrile. The force field for the solvent follows the parametrization of Guàrdia *et al.*[47], which is based on a rigid linear three-site model. Details of the implementation of the pairwise potential for acetonitrile in ASE are presented in the ESI. The chosen ace-

tonitrile model is based on fixed-value point charges, thus the QM/MM coupling does not include the polarization of the solvent induced by the electronic density of the QM subsystem. This contribution can be important for accurately predicting processes where the fast electronic response of the solvent to changes in the QM density plays a large role, such as when calculating absorption spectra[48]. Conversely, for the phenomena studied here, the magnitude and time scales of the structural distortions of the solute allow for nuclear rearrangement within the solvent. This type of reorganization is expected to dominate the total solvent response, which, therefore, can be described by displacements of fixed charges of the solvent molecules without significant loss of accuracy[49,50].

The QM/MM setup consists of $[Cu(dmphen)_2]^+$ and 468 acetonitrile molecules in a cubic box with side length of 35 Å, where the QM subsystem includes only the complex. Nonelectrostatic nonbonded interactions between the QM atoms and MM sites are modeled through a Lennard-Jones (LJ) potential with parameters taken from the universal force field (UFF)[51].

Initial positions and velocities for the nonequilibrium excited-state trajectories are drawn from a statistically significant number of ground-state configurations equilibrated at 300 K. To generate the S_0 QM/MM thermal equilibrium ensemble, we first equilibrate the system in the ground state at 300 K using a Langevin thermostat[52] with 1 fs time step and then continue the propagation with 2 fs time step applying the thermostat only to the solvent. During the dynamics, the internal geometry of the acetonitrile molecules is fixed by applying holonomic constraints for linear triatomic molecules from Ciccotti *et al.*[53] (see the ESI). To ensure further stability to the simulations, we fix two bond lengths per hydrogen atom of the complex using the implementation of RATTLE in ASE[54]. These constraints do not affect the flattening dynamics nor the correlation between the flattening and the rotation of the methyl groups as confirmed by test trajectories in vacuum. After obtaining a sufficiently long equilibrated trajectory (∼12 ps), to accelerate the data collection we start further 25 trajectories from frames of the first by imposing a Maxwell-Boltzmann distribution at 300 K to the initial momenta. In total, we collected ∼65000 ground-state QM/MM equilibrated frames (∼130 ps). The S1 QM/MM and gas-phase trajectories are propagated in 48 parallel runs for both cases, for a total of 280 and 260 ps respectively, and use the same BOMD parameters and QM/MM setup as in the production ground-state simulations. More details on the generation of initial conditions for the excited-state trajectories are reported in section 4 of the ESI.

For the calculation of the minimum energy path (MEP), we use the nudged elastic band (NEB) method[55,56] with climbing image[57] and improved tangent estimate[58], as implemented in ASE. The initial and final images, corresponding to the perpendicular and flattened geometries of $[Cu(dmphen)_2]^+$ in the S_1 state, are first fully optimized in vacuum and then interpolated with the IDPP method[59] to generate 10 intermediate images. The convergence criterion for all geometry optimizations is a maximum atomic force smaller than 0.02 eV/Å.

3 Results

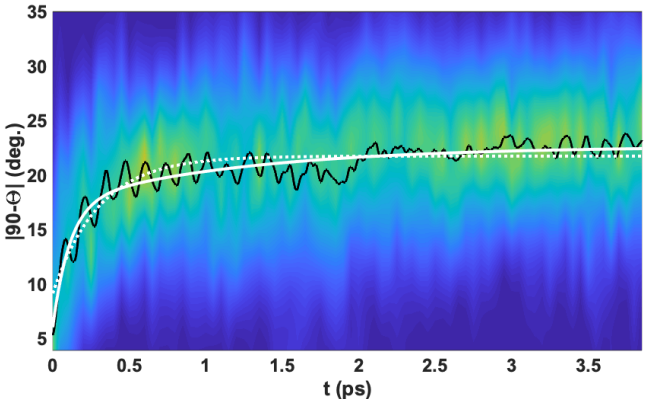

Fig. 2 Density plot of the evolution of the distribution of angles Θ (see Figure 1) obtained from the nonequilibrium QM/MM trajectories of $[Cu(dmphen)_2]^+$ in the S_1 state in acetonitrile. The bins for the sampling are 50 fs by 1.5 deg. The ligands rotate clockwise or anticlockwise. The black curve is the instantaneous average of $|90^\circ - \Theta|$, while the dotted and continuous white curves are monoexponential and biexponential fits, respectively.

The flattening dynamics of the excited-state population in solution is analyzed in Figure 2 through the evolution of the distribution of interligand dihedral angles Θ. The absolute deviation of Θ from 90° averaged over all S_1 trajectories can be fitted with a single exponential function with a time constant of 300 ± 14 fs. This value is in good agreement with the 340 fs decay time inferred by Tahara *et al.*[7] from time-resolved emission measurements. On the other hand, the instantaneous average $|90^\circ - \Theta|$ from our simulations can also be fitted with a biexponential function delivering time constants of 110 ± 12 fs and 1.2 ± 0.2 ps, the fast component being consistent with the experimental observation of Chen *et al.*[19], who attributed to the flattening a time scale of ∼100 fs from fluorescence upconversion measurements. In the following, we show that in order to select a correct model for the flattening dynamics and unambiguously assign its time scales, we need to consider the dynamical response of the solvent to photoexcitation of the complex.

In Figure 3 we examine the solute-solvent pairwise radial distribution functions (RDFs) of the atomic distances between Cu and the acetonitrile molecules sampled from the thermally equilibrated S_0 and S_1 QM/MM trajectories. Comparing the RDFs of the Cu-N distances (Figure 3, Left) with those of the Cu-C and Cu-Methyl distances (Figure 3, Right), reveals the preferential orientation of solvent molecules with the N atoms towards the metal, both in the ground and excited states. The small amplitude and broadness of the first peak of the ground-state Cu-N RDF, around ∼5 Å, are indicative of a low degree of ordering in the solvation shell closest to the metal. In the excited state this peak almost entirely disappears, while the amplitude at $r(\mathrm{Cu-N}) < 4.75$ Å becomes considerably bigger. These changes in the solute-solvent RDFs imply that there is a higher probably to find acetonitrile molecules closer to Cu (3 Å $< r(\mathrm{Cu-N}) < 4.75$ Å) after structural relaxation in the S_1

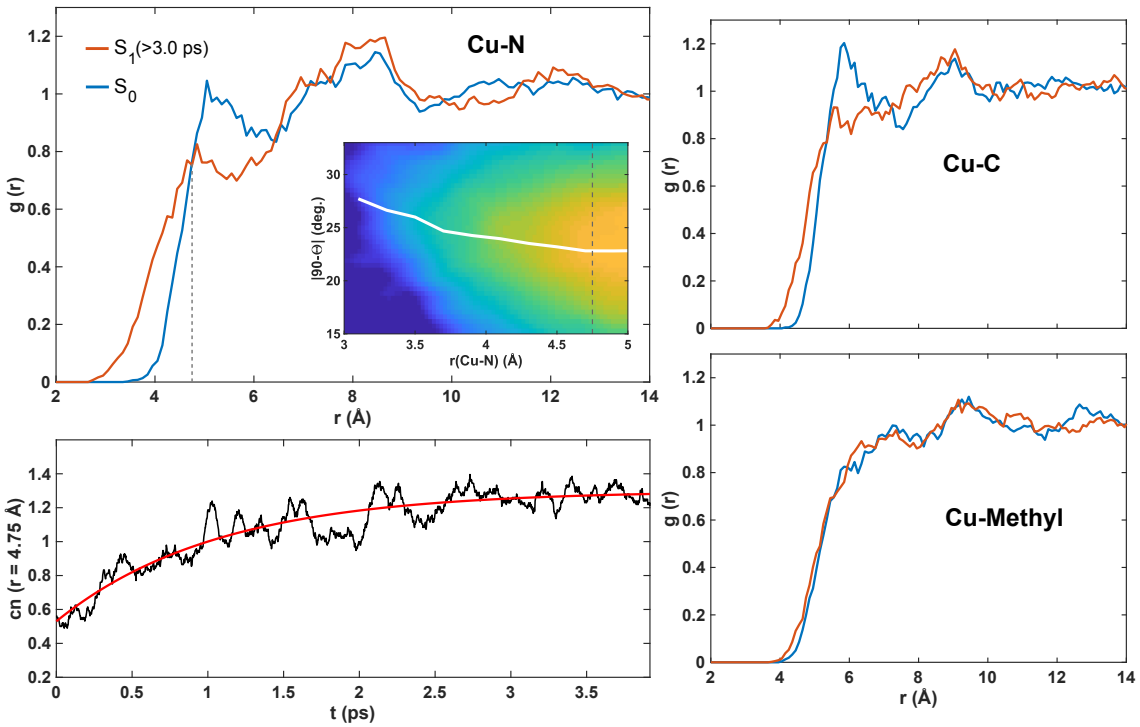

Fig. 3 (Left, top), (Right) RDFs of the atomic distances between Cu and the acetonitrile molecules sampled from the QM/MM ensemble of $[Cu(dmphen)_2]^+$ in the ground state at 300 K and from the S_1 QM/MM trajectories after structural relaxation of the solute. The inset shows the density plot of the joint probability distribution of flattening angles Θ and Cu-N distances of solvent molecules in the first solvation shell of the complex in the S_1 state, together with the mean $|90^\circ - \Theta|$ for a given $r(\mathrm{Cu-N})$ (white curve). The conditional distribution of Θ angles shows a shift to larger values for $r(\mathrm{Cu-N}) < 4.75$ Å. (Left, Bottom) Time evolution of the Cu-N cumulative coordination number at $r(\mathrm{Cu-N}) = 4.75$ Å (indicated by the dashed vertical line in the top panel). The red curve represents a fit with a monoexponential function.

state, consistent with the MLCT nature of the electronic transition and the fact that the flattening distortion leaves more space between the ligands for solvent molecules to approach the metal center. The interaction between solvent molecules and the excited state of $[Cu(dmphen)_2]^+$ is weak since the approach to Cu is only to within 3 to 4.75 Å, and no new distinct peak is observed at such distances in the Cu-N RDF. Therefore, the solvent does not coordinate the metal to form a solute-solvent exciplex. This confirms the observations of Penfold *et al.* [10] from previous classical and QM/MM MD simulations.

Here, we further characterize the dynamics of the solvent in the first solvation shell and examine possible correlations with the flattening. To this end, we consider the time evolution of the Cu-N cumulative coordination number after excitation. We find that the cumulative coordination number at a Cu-N distance of 4.75 Å exhibits dynamics with a time constant of 1.06 ± 0.05 ps as revealed by an exponential fit (see Figure 3). Notably, this time scale is similar to the slow component of the biexponential fit of the flattening dynamics shown in Figure 2. To test if the approach of the solvent to the metal is coupled to the degree of flattening of the ligands, we construct the joint probability distribution of flattening angles and Cu-N distances sampled from all the S_1 trajectory considering acetonitrile molecules found in the first coordination shell around Cu. The shape of the distribution, shown as a density plot in the inset of Figure 3, clearly reveals that when acetonitrile molecules are closer to the metal, $[Cu(dmphen)_2]^+$ is more likely to be found in a configuration with a larger flattening angle. This observation points to a correlation between the extent of the flattening and the distance of solvent molecules to Cu.

To shed further light on the effect that the interaction between solvent molecules and Cu has on the flattening dynamics, we perform additional excited-state nonequilibrium BOMD simulations of the complex in vacuum by starting gas-phase S_1 trajectories from the same positions and velocities employed as initial conditions in the QM/MM BOMD simulations (hence the temperature of the complex is still 300 K). Figure 4 shows the instantaneous average $|90^\circ - \Theta|$ obtained from the gas-phase trajectories. The flattening dynamics in vacuum appears different than in solution on long time scale. We estimate the rate of flattening in vacuum by fitting the average $|90^\circ - \Theta|$ with a monoexponential function, as also done by Agena *et al.* [30] for the gas-phase dynamics of the parent compound $[Cu(phen)_2]^+$ simulated using semiglobal PESs. The fit delivers a time constant of 90 ± 16 fs. Significantly, the initial fast relaxation along the flattening coordinate in vacuum parallels the fast rate obtained from the biexponential fit in acetonitrile. On the other hand, at long time scale, after this prompt rise, the interligand dihedral angles show highly harmonic coherent oscillations with a period of ∼1 ps

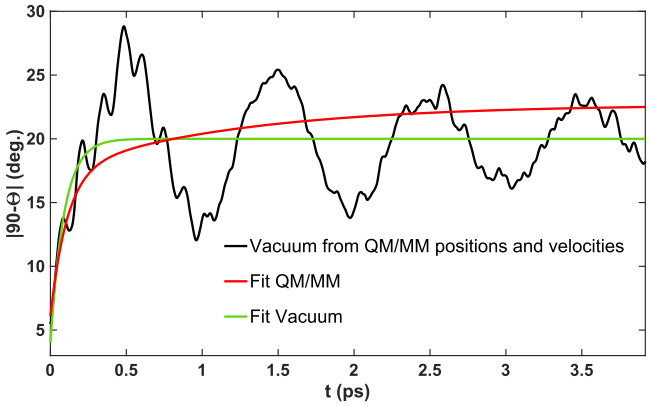

Fig. 4 Time evolution of the deviation from 90° of the flattening angle Θ averaged over the nonequilibrium S_1 trajectories collected in vacuum (black curve), together with a monoexponential fit to it (green curve) and the biexponential fit (red curve) to the average from the S_1 trajectories in acetonitrile already shown in Figure 2.

that survive for longer than 4 ps, due to lack of damping by the solvent. The oscillations occur around an approximately constant value of 20°, while in solvent (see Figure 2) the average $|90^\circ - \Theta|$ grows monotonically towards a value around ∼3° bigger than in vacuum. Analysis of the solvent response and comparison between the evolution of the flattening angles in vacuum and in solution seem to suggest a different flattening dynamics on short and long time scales in acetonitrile. The possibility of a two-step flattening dynamics in solution will be further explored in the next section.

By comparing the simulations in solution and in vacuum, we can also elucidate the role of the methyl groups in the relaxation along the flattening coordinate in the S_1 state. Figure 5 shows polar histograms of all HCCN methyl dihedral

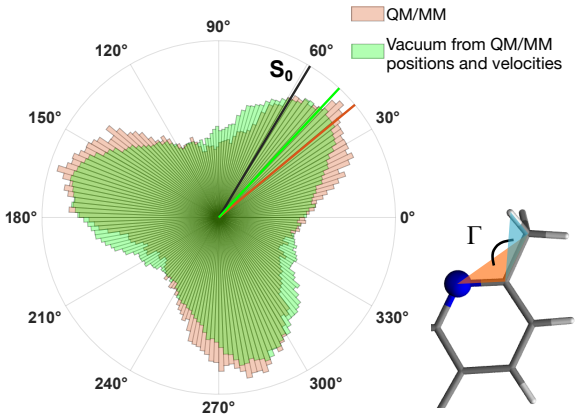

Fig. 5 Polar distributions of the HCCN methyl dihedral angles (Γ) in $[Cu(dmphen)_2]^+$ obtained from the S_1 QM/MM (red) and gas-phase (green) trajectories. The lines represent the average of the distributions considering only the peaks at lower angles (the black line is the average of the ground-state distribution shown in Figure S8 of the ESI). The distributions sample Γ angles of only the ensemble of molecules with the ligands rotated clockwise with respect to the perpendicular geometry.

angles Γ of the complex sampled from both the S_1 QM/MM and vacuum trajectories. The distributions illustrate that Γ can assume a broad range of values, which implies that at 300 K the thermal energy available is enough to allow rotation of the methyl groups around their C_3 symmetry axes. On the other hand, the methyls retain preferred orientations characterized by the values at which the distributions peak. In the ground state (see Figure S8 in the ESI for the S_0 distribution), the preferred configuration has dihedral angles of ∼60°, 180° and 300°, with a periodicity given by the methyl group geometry. In the S_1 state in vacuum, the orientation of the methyl groups shows a deviation of ∼13° from that of the ground state. Rotation of the methyl groups in the excited state reduces steric hindrance at the flattened geometry. Significantly, in solvent the deviation appears ∼7° bigger, and the respective distribution narrower. This different behavior in solvent can be explained by the fact that the flattening distortion is bigger in acetonitrile than in vacuum, as previously seen, thereby requiring further rotation of the methyl groups.

The results presented so far indicate that in the S_1 relaxation of $[Cu(dmphen)_2]^+$ there is a correlation between the magnitude of the flattening and rotation of the methyl substituents. In the following, we characterize in more detail the coupling between relaxation along the coordinates Θ and Γ, representing the flattening distortion and rotation of the methyl groups around their C_3 symmetry axes, respectively. In particular, we investigate whether the rotation of the substituents promotes the flattening or the molecule in the S_1 state at the perpendicular geometry can change its structure directly along the flattening coordinate. At the same time, we test the existence of an energy barrier between the perpendicular and flattened geometries in S_1. To this end, in Figure 6 we analyze the calculated excited-state minimum energy path (MEP) between the S_1 perpendicular and flattened geometries. No barrier between the initial and final structures is observed along the MEP, and the perpendicular geometry is a saddle point on the S_1 PES, as is also confirmed by a normal mode analysis carried out at this geometry. Figure 6 also shows the deviation from 90° of the flattening angle Θ and the average of the methyl rotational dihedral angles Γ along the MEP. A correlation between the magnitude of $|90^\circ - \Theta|$ and Γ is manifested for deviations from the perpendicular geometry bigger than ∼15°. For smaller values of $|90^\circ - \Theta|$, the methyl groups do not significantly rotate from the orientation at the perpendicular configuration (the positive deviation from 60° of Γ that is observed at $|90^\circ - \Theta| < 15^\circ$ is a consequence of a misalignment of the N1-N1′ and N2-N2′ axes with respect to the methyl C_3 symmetry axes that characterizes the flattened geometries, and not of a rotation of the methyl groups around the C_3 axes). The NEB calculations demonstrate that the complex can assume flattened configurations even if the methyl groups do not rotate. Rotation of the substituents is required for distortions from the perpendicular geometry larger than 15° and to eventually achieve the S_1 minimum energy structure.

In Figure 7 we present the evolution of the flattening angle Θ and methyl rotational dihedral angles Γ along a sin-

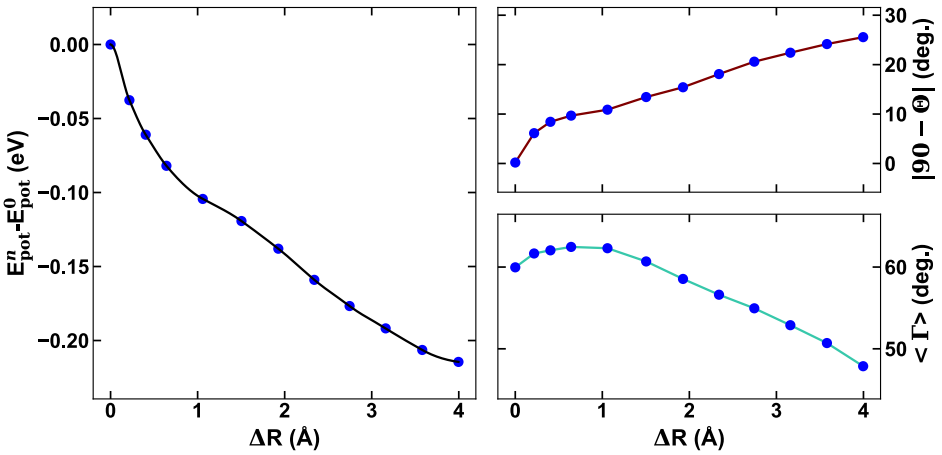

Fig. 6 (Left) Minimum energy path (MEP) from the perpendicular to the flattened geometry of $[Cu(dmphen)_2]^+$ in the S_1 excited state computed in vacuum using the NEB method. Image $n = 0$ is the saddle point on the vacuum S_1 PES found at the perpendicular configuration of the ligands. (Right) Deviation from 90° of the interligand angle Θ (top) and average of the HCCN methyl dihedral angles (bottom) along the MEP. The reaction coordinate is given as a cumulative displacement of the atoms with respect to the perpendicular structure ($\Delta R_n = \sum_{i=1}^{n} \sqrt{\sum_{j=1}^{3N} (q_j^i - q_j^{i-1})^2}$, for images $n > 0$, where N is the total number of atoms in the complex and q_j are the atomic cartesian coordinates).

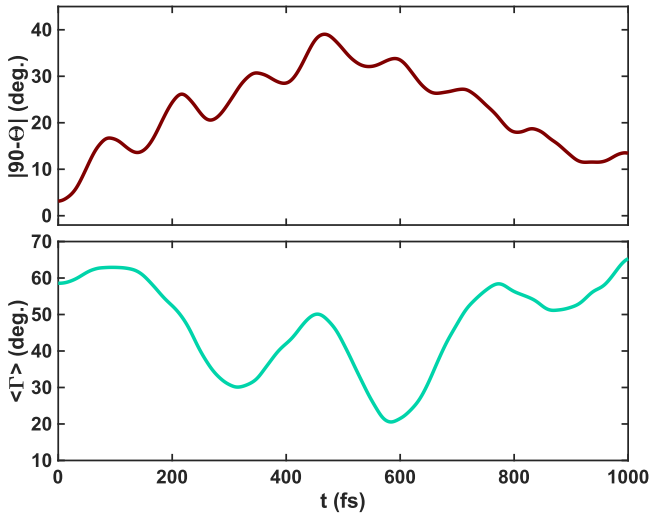

Fig. 7 Evolution of the deviation from 90° of the flattening angle (top) and average of the HCCN methyl rotational dihedral angles (bottom) along a single trajectory propagated in vacuum in the S_1 state starting from the gas-phase optimized geometry of $[Cu(dmphen)_2]^+$ in the ground state.

gle S_1 trajectory propagated in vacuum starting from the gas-phase optimized ground-state geometry of $[Cu(dmphen)_2]^+$. The molecule starts flattening immediately after excitation. Henceforth, the evolution of the flattening angle Θ is characterized by large amplitude oscillations around the equilibrium value of ∼ 70°. Here, we focus on the first 1 ps after excitation, corresponding approximately to the time when one oscillation along the flattening coordinate is completed. As seen from Figure 7, rotation of the methyl groups starts after ∼160 fs, when the flattening angle has reached a value of around 15° (the positive deviation from 60° before 160 fs is caused by a misalignment of the N1-N1′ and N2-N2′ axes with respect to the methyl C_3 symmetry axes for flattened configurations when the methyl groups do not rotate, as also observed in the MEP in Figure 6). The angles Γ exhibit the largest deviation from the ground-state equilibrium value at around 550 fs, i.e. when the molecule has reached the first outer turning point in the oscillation along the flattening coordinate, corresponding to the largest distortion from the perpendicular configuration. These observations indicate that rotation of the methyl groups occurs to achieve large flattening distortions ($\Theta > 15°$) by reducing steric hindrance, but it does not promote the initial motion along the flattening coordinate, as also deduced from the analysis of the MEP.

4 Discussion

Ultrafast experimental studies of $[Cu(dmphen)_2]^+$ in solution have previously assumed a single time constant for the flattening distortion in the excited state; however, the lack of agreement among the proposed experimental values calls for a test of this assumption. The results presented in the previous section allow us to assess the validity of a two-step model of the flattening dynamics in acetonitrile.

First of all, analysis of the time dependence of the solute-solvent RDFs highlights the similarity between the time scale of the rise of the Cu-N RDF at short distances ($r(Cu-N) < 4.75$ Å) and the slow component of a biexponential fit of the evolution of the flattening angles in solution. Secondly, the comparison between the evolution of the flattening angles from the gas-phase and QM/MM BOMD simulations shows that (i) both in vacuum and in solution there is a prompt rise with an exponential rate of ∼100 fs, and (ii) the long-time dynamics in vacuum is different than in solution: while the gas-phase equilibrium flattening angle stabilizes around a value of 70° at ∼500 fs, in solution the flattening angle keeps growing monotonically towards larger values. Lastly, residual analysis and likelihood-ratio tests are used to verify that a biexponential model gives a significantly better fit of the evolution of

the flattening angles obtained from the excited-state QM/MM simulations (Figure 2) than a monoexponential model. The residuals of the monoexponential and biexponential fits are shown in Figures S5 and S6 of the ESI. The residuals of the biexponential fit are smaller over almost the entire time interval, which means that the quality of the fit is considerably improved with respect to the model with fewer parameters, as also indicated a by 10% bigger R^2 value (see Table S2 in the ESI). To confirm that the improvement of the quality of the fit upon the use of additional parameters in the model is statistically significant, we carry out an F-test[60,61], which involves computing:

$$F = \frac{(RSS_1 - RSS_2)(k - p_2 - 1)}{RSS_2(p_2 - p_1)}$$

where k is the number of data points, RSS_1 and RSS_2 are the residual sum of squares of the monoexponential and biexponential fits, respectively, and p_1 and p_2 the number of parameters of the two models. We then integrate the F-distribution with $p_2 - p_1$ and $k - p_2 - 1$ degrees of freedom above the value of F found from the equation above to obtain the probability that the improvement of the quality of the fit when adding more parameters to the model is due to chance[60]. The calculated probability is negligible.

All the above observations are clear indications that the flattening dynamics of $[Cu(dmphen)_2]^+$ in acetonitrile from our simulations is a two-step process. At short time scale (t < 500 fs), the structural distortion appears solvent independent to a large extent; while on longer time scale, acetonitrile molecules approaching the metal center induce an additional, slower flattening. The interaction between Cu and closely approaching acetonitrile molecules is only labile as implied by the lack of structuring in the solute-solvent RDFs, but enough to exert strain on the ligands to flatten to a further extent.

The findings of the present work on the mechanism of photoinduced structural flattening of $[Cu(dmphen)_2]^+$ in acetonitrile can be summarized as follows: (i) the complex undergoes a prompt flattening (∼110 fs time constant), which is not affected by the presence of solvent molecules; (ii) as the deviation from ∼90° of the flattening angle reaches a value of ∼20°, acetonitrile molecules come closer to Cu (3 Å $< r(Cu-N) <$ 4.75 Å) inducing a further angular distortion on a ∼1 ps time scale; (iii) while there is no energy barrier between the perpendicular and flattened geometries and the flattening does not require rotation of the methyl groups to be promoted, a correlation between the extent of the flattening and rotation of the methyls exists for flattening distortions bigger than ∼15°; (iv) due to this correlation and to the enhanced flattening distortion caused by the approach of solvent molecules to Cu, in acetonitrile the methyl groups rotate of a larger angle than in vacuum. We note that the time scales of the flattening extracted from the nonequilibrium QM/MM BOMD simulations in the present work can be considered an upper limit of the time constants that can be observed from ultrafast experiments performed with photoexcitation to a singlet MLCT state higher in energy than S_1. This is because although no significant flattening dynamics occurs in high-lying S_n states, as evidenced by PES and quantum dynamics calculations[9,34], the wavepacket can still spread and that will lead to a a faster flattening distortion after IC to S_1.

Agena *et al.*[30] have previously reported nonequilibrium MD simulations on excited-state PESs of $[Cu(phen)_2]^+$ in acetonitrile, showing that strong coordination between solvent molecules and the complex can lead to a slow, ps-long flattening distortion. Our results establish that transiently approaching acetonitrile molecules can have a similar effect on the excited-state flattening dynamics of the methyl-substituted $[Cu(dmphen)_2]^+$ complex.

In agreement with the picture of photoinduced flattening in $[Cu(dmphen)_2]^+$ proposed by Tahara *et al.*[6,7,15,18] based on ultrafast optical experiments in dichloromethane, our simulations predict that rotation of the methyl groups on the phenanthroline ligands is necessary to reduce steric hindrace while the ligands flatten in the excited state. Here, we shed new light on the nature of the coupling between these two intramolecular motions by showing that while the methyls need to rotate to achieve deviations from the perpendicular configuration bigger than ∼15°, smaller angular distortions of the ligands are not activated by this motion of the substituent groups. This correlation is particularly important in the presence of a donor solvent such as acetonitrile, in which the approach of solvent molecules to Cu induces a bigger flattening distortion than in vacuum.

5 Conclusions

Using statistically robust BOMD simulations of $[Cu(dmphen)_2]^+$ in the lowest singlet MLCT excited state with explicit QM/MM description of the solvent, we provide the first theoretical assignment of the time scales of the photoinduced flattening motion of the complex in acetonitrile. This is enabled by comparison of the evolution of the nonequilibrium ensemble of molecules in solution with trajectories propagated in vacuum and by analysis of the excited-state MEP. The time scales of the flattening are determined by a mechanism of two-step concerted solute-solvent structural dynamics: initial fast (∼110 fs) flattening is followed by the approach of acetonitrile molecules to the open metal center; this in turn induces a further angular distortion of the ligands on a ∼1 ps time scale and rotation of the methyl groups to reduce steric hindrance.

The present work demonstrates that the photoinduced structural dynamics of Cu(I) bis-phenanthroline complexes can be strongly coupled to the dynamics of the solvent and depend on conformational effects. Similar manifestations of solvent and structural dependence in the excited-state dynamics of photofunctional transition metal complexes are being discovered with increasing frequency[49,50,62–64]. It is important to account for explicit solvent effects and vibrational sampling at finite temperature for low-energy modes[65,66] when formulating mechanistic hypothesis to explain experimental trends. These considerations are particularly relevant in studies aimed at accelerating the development of next-generation

light-converting materials based on Earth-abundant metal compounds.

Conflicts of interest

There are no conflicts to declare.

Acknowledgements

The present work has received funding from the Icelandic Research Fund (grants number 196070-051 and 196279-051). The authors are grateful to Aleksei Ivanov for support with the NEB calculations and Ask H. Larsen for discussion about the implementation of the acetonitrile force field in ASE.

Notes and references

1 Y. Zhang, M. Schulz, M. Wächtler, M. Karnahl and B. Dietzek, *Coordination Chemistry Reviews*, 2018, **356**, 127–146.

2 M. W. Mara, K. A. Fransted and L. X. Chen, *Coordination Chemistry Reviews*, 2014, **282-283**, 2–18.

3 N. Armaroli, *Chemical Society Reviews*, 2001, **30**, 113–124.

4 D. V. Scaltrito, D. W. Thompson, J. A. O'Callaghan and G. J. Meyer, *Coordination Chemistry Reviews*, 2000, **208**, 243–266.

5 R. S. Khnayzer, C. E. McCusker, B. S. Olaiya and F. N. Castellano, *Journal of the American Chemical Society*, 2013, **135**, 14068–14070.

6 M. Iwamura, H. Watanabe, K. Ishii, S. Takeuchi and T. Tahara, *Journal of the American Chemical Society*, 2011, **133**, 7728–7736.

7 M. Iwamura, S. Takeuchi and T. Tahara, *J. Am. Chem. Soc*, 2007, **129**, 5248–5256.

8 C. T. Cunningham, J. J. Moore, K. L. H. Cunningham, P. E. Fanwick and D. R. Mcmillin, *Inorg. Chem.*, 2000, **39**, 3638–3644.

9 G. Capano, U. Rothlisberger, I. Tavernelli and T. J. Penfold, *Journal of Physical Chemistry A*, 2015, **119**, 7026–7037.

10 T. J. Penfold, S. Karlsson, G. Capano, F. A. Lima, J. Rittmann, M. Reinhard, M. H. Rittmann-Frank, O. Braem, E. Baranoff, R. Abela, I. Tavernelli, U. Rothlisberger, C. J. Milne and M. Chergui, *Journal of Physical Chemistry A*, 2013, **117**, 4591–4601.

11 Z. A. Siddique, Y. Yamamoto, T. Ohno and K. Nozaki, *Inorganic Chemistry*, 2003, **42**, 6366–6378.

12 E. Mejía, S. P. Luo, M. Karnahl, A. Friedrich, S. Tschierlei, A. E. Surkus, H. Junge, S. Gladiali, S. Lochbrunner and M. Beller, *Chemistry - A European Journal*, 2013, **19**, 15972–15978.

13 N. A. Gothard, M. W. Mara, J. Huang, J. M. Szarko, B. Rolczynski, J. V. Lockard and L. X. Chen, *Journal of Physical Chemistry A*, 2012, **116**, 1984–1992.

14 S. Garakyaraghi, P. Koutnik and F. N. Castellano, *Physical Chemistry Chemical Physics*, 2017, **19**, 16662–16668.

15 M. Iwamura, S. Takeuchi and T. Tahara, *Phys. Chem. Chem. Phys.*, 2014, **16**, 4143–4154.

16 S. Tschierlei, M. Karnahl, N. Rockstroh, H. Junge, M. Beller and S. Lochbrunner, *ChemPhysChem*, 2014, **15**, 3709–3713.

17 S. Garakyaraghi, E. O. Danilov, C. E. McCusker and F. N. Castellano, *The Journal of Physical Chemistry A*, 2015, **119**, 3181–3193.

18 M. Iwamura, S. Takeuchi and T. Tahara, *Accounts of Chemical Research*, 2015, **48**, 782–791.

19 G. B. Shaw, C. D. Grant, H. Shirota, E. W. C. Jr, G. J. Meyer and L. X. Chen, *J. Am. Chem. Soc*, 2007, **129**, 2147–2160.

20 L. X. Chen, G. B. Shaw, I. Novozhilova, T. Liu, G. Jennings, K. Attenkofer, G. J. Meyer and P. Coppens, *Journal of the American Chemical Society*, 2003, **125**, 7022–7034.

21 T. Katayama, T. Northey, W. Gawelda, C. J. Milne, G. Vankó, F. A. Lima, R. Bohinc, Z. Németh, S. Nozawa, T. Sato, D. Khakhulin, J. Szlachetko, T. Togashi, S. Owada, S.-i. Adachi, C. Bressler, M. Yabashi and T. J. Penfold, *Nature Communications*, 2019, **10**, 3606.

22 M. S. Kelley, M. L. Shelby, M. W. Mara, K. Haldrup, D. Hayes, R. G. Hadt and X. Zhang, *J Physics B: At. Mol. Phys.*, 2017, **50**, 154006.

23 M. Iwamura, F. Kobayashi and K. Nozaki, *Chemistry Letters*, 2016, **45**, 167–169.

24 L. X. Chen, G. Jennings, T. Liu, D. J. Gosztola, J. P. Hessler, D. V. Scaltrito and G. J. Meyer, *J. Am. Chem. Soc*, 2002, **124**, 10861–10867.

25 M. K. Eggleston, D. R. McMillin, K. S. Koenig and A. J. Pallenberg, *Inorganic Chemistry*, 1997, **36**, 172–176.

26 D. R. McMillin, J. R. Kirchhoff and K. V. Goodwin, *Coordination Chemistry Reviews*, 1985, **64**, 83–92.

27 M. W. Blaskie and D. R. Mcmillin, *Inorganic Chemistry*, 1980, **19**, 3519–3522.

28 S. L. Du and Z. Lan, *Physical Chemistry Chemical Physics*, 2016, **18**, 7641–7650.

29 G. Capano, T. J. Penfold, M. Chergui and I. Tavernelli, *Phys. Chem. Chem. Phys.*, 2017, **19**, 19590–19600.

30 A. Agena, S. Iuchi and M. Higashi, *Chemical Physics Letters*, 2017, **679**, 60–65.

31 G. Capano, M. Chergui, U. Rothlisberger, I. Tavernelli and T. J. Penfold, *The journal of physical chemistry. A*, 2014, **118**, 9861–9869.

32 M. Schulz, C. Reichardt, C. Müller, K. R. Schneider, J. Holste and B. Dietzek, *Inorganic Chemistry*, 2017, **56**, 12978–12986.

33 L. Hua, M. Iwamura, S. Takeuchi and T. Tahara, *Phys. Chem. Chem. Phys.*, 2015, **17**, 2067–2077.

34 G. Capano, T. J. Penfold, U. Röthlisberger and I. Tavernelli, *CHIMIA International Journal for Chemistry*, 2014, **68**, 227–230.

35 A. D. Becke, *Physical Review A*, 1988, **38**, 3098.

36 C. Lee, W. Yang and R. G. Parr, *Physical Review B*, 1988, **37**, 785–789.

37 A. H. Larsen, M. Vanin, J. J. Mortensen, K. S. Thygesen and K. W. Jacobsen, *Phys. Rev. B*, 2009, **80**, 195112.

38 J. Enkovaara, C. Rostgaard, J. J. Mortensen, J. Chen, M. Dulak, L. Ferrighi, J. Gavnholt, C. Glinsvad, V. Haikola,

H. A. Hansen, H. H. Kristoffersen, M. Kuisma, A. H. Larsen, L. Lehtovaara, M. Ljungberg, O. Lopez-Acevedo, P. G. Moses, J. Ojanen, T. Olsen, V. Petzold, N. A. Romero, J. Stausholm-Møller, M. Strange, G. A. Tritsaris, M. Vanin, M. Walter, B. Hammer, H. Häkkinen, G. K. H. Madsen, R. M. Nieminen, J. K. Nørskov, M. Puska, T. T. Rantala, J. Schiøtz, K. S. Thygesen and K. W. Jacobsen, *Journal of Physics: Condensed matter*, 2010, **22**, 253202.

39 J. Mortensen, L. Hansen and K. W. Jacobsen, *Physical Review B*, 2005, **71**, 035109.

40 M. Abedi, G. Levi, D. B. Zederkof, N. E. Henriksen, M. Pápai and K. B. Møller, *Phys. Chem. Chem. Phys.*, 2019, **21**, 4082–4095.

41 G. Levi, M. Papai, N. E. Henriksen, A. O. Dohn and K. B. Møller, *Journal of Physical Chemistry C*, 2018, **122**, 7100–7119.

42 G. Levi, *Ph.D. thesis*, Technical University of Denmark, 2018.

43 B. Himmetoglu, A. Marchenko, I. Dabo and M. Cococcioni, *Journal of Chemical Physics*, 2012, **137**, 154309.

44 A. O. Dohn, E. O. Jónsson, G. Levi, J. J. Mortensen, O. Lopez-Acevedo, K. S. Thygesen, K. W. Jacobsen, J. Ulstrup, N. E. Henriksen, K. B. Møller and H. Jónsson, *Journal of Chemical Theory and Computation*, 2017, **13**, 6010–6022.

45 A. H. Larsen, J. J. Mortensen, J. Blomqvist, I. E. Castelli, R. Christensen, M. Dułak, J. Friis, M. N. Groves, B. Hammer, C. Hargus, E. D. Hermes, P. C. Jennings, P. B. Jensen, J. Kermode, J. R. Kitchin, E. L. Kolsbjerg, J. Kubal, K. Kaasbjerg, S. Lysgaard, J. B. Maronsson, T. Maxson, T. Olsen, L. Pastewka, A. Peterson, C. Rostgaard, J. Schiøtz, O. Schütt, M. Strange, K. S. Thygesen, T. Vegge, L. Vilhelmsen, M. Walter, Z. Zeng and K. W. Jacobsen, *Journal of Physics: Condensed Matter*, 2017, **29**, 273002.

46 S. R. Bahn and K. W. Jacobsen, *Computing in Science & Engineering*, 2002, **4**, 55.

47 E. Guardia, R. Pinzón, J. Casulleras, M. Orozco and F. J. Luque, *Molecular Simulation*, 2001, **26**, 287.

48 Q. Li, B. Mennucci, M. A. Robb, L. Blancafort and C. Curutchet, *Journal of Chemical Theory and Computation*, 2015, **11**, 1674–1682.

49 A. O. Dohn, E. O. Jónsson, K. S. Kjær, T. B. van Driel, M. M. Nielsen, K. W. Jacobsen, N. E. Henriksen and K. B. Møller, *Journal of Physical Chemistry Letters*, 2014, **5**, 2414–2418.

50 T. B. Driel, K. S. Kjær, R. Hartsock, A. O. Dohn, T. Harlang, M. Chollet, M. Christensen, G. Wojciech, N. E. Henriksen, J. G. Kim, K. Haldrup, K. H. Kim, H. Ihee, J. Kim, H. Lemke, Z. Sun, V. Sundstrom, W. Zhang, D. Zhu, K. B. Møller, M. M. Nielsen and K. J. Gaffney, *Nature Communications*, 2016, **7**, 13678.

51 A. Rappe, C. Casewit, K. Colwell, W. G. III and W. Skiff, *Journal of the American Chemical Society*, 1992, **114**, 10024–10035.

52 E. Vanden-Eijnden and G. Ciccotti, *Chemical Physics Letters*, 2006, **429**, 310–316.

53 G. Ciccotti, M. Ferrario and J.-P. Ryckaert, *Molecular Physics*, 1982, **47**, 1253–1264.

54 H. C. Andersen, *Journal of Computational Physics*, 1983, **52**, 24.

55 V. Ásgeirsson and H. Jónsson, in *Exploring Potential Energy Surfaces with Saddle Point Searches*, ed. W. Andreoni and S. Yip, Springer International Publishing, 2018.

56 H. Jónsson, G. Mills and K. W. Jacobsen, in *Nudged elastic band method for finding minimum energy paths of transitions*, ed. B. J. Berne, G. Ciccotti and D. F. Coker, World Scientific, 1998, ch. 16, pp. 385–404.

57 G. Henkelman, B. P. Uberuaga and H. Jónsson, *The Journal of Chemical Physics*, 2000, **9901**, 9901.

58 G. Henkelman and H. Jónsson, *Journal of Chemical Physics*, 2000, **113**, 9978–9985.

59 S. Smidstrup, A. Pedersen, K. Stokbro and H. Jónsson, *The Journal of Chemical Physics*, 2014, **140**, 214106.

60 K. B. Anderson and J. A. Conder, *Energy and Fuels*, 2011, **25**, 1578–1584.

61 G. S. Maddala and K. Lahiri, *Introduction to Econometrics*, Wiley, 4th edn., 2009.

62 C. Daniel, E. Gindensperger and M. Fumanal, *Physical Chemistry Chemical Physics*, 2017, **20**, 1134–1141.

63 A. O. Dohn, K. S. Kjær, T. B. Harlang, S. E. Canton, M. M. Nielsen and K. B. Møller, *Inorganic Chemistry*, 2016, **55**, 10637–10644.

64 A. E. Nahhas, A. Cannizzo, F. V. Mourik, A. M. Blanco-Rodríguez, S. Záliš, A. Vlček and M. Chergui, *Journal of Physical Chemistry A*, 2010, **114**, 6361–6369.

65 S. Mai, H. Gattuso, A. Monari and L. González, *Frontiers in Chemistry*, 2018, **6**, year.

66 M. Barbatti and K. Sen, *International Journal of Quantum Chemistry*, 2016, **116**, 762–771.